THE AMERICAN SOCIETY OF MECHANICAL ENGINEERS
345 E. 47th St., New York, N.Y. 10017

98-GT-558

PREDICTED INFLUENCE OF INTAKE ACOUSTICS UPON PART-SPEED FAN FLUTTER

J. W. Chew[1], M. Vahdati[2] & M. Imregun[2]

[1]Rolls-Royce plc., Moor Lane, Derby DE2 8BJ, UK
[2]Imperial College, MED, London SW7 2BX, UK

ABSTRACT

While it is known that the occurrence of flutter is dominated by aerodynamics, it also depends on such parameters as inlet distortion and acoustics, aerodynamic and mechanical mistuning, and structural damping. It is shown in this paper that recent developments in predictive methods are showing considerable promise and leading to an improved understanding of the controlling parameters. A non-linear coupled structural-fluid approach is described and applied at engine representative conditions. This involves 3D unsteady CFD calculations of the fan and intake flows. Particular emphasis is placed on the influence of intake acoustics. Earlier work on flutter prediction has focused on either the fan assembly without a proper representation of the intake, or the calculation of the acoustic properties of the intake without properly representing the interaction with the fan. The present study includes a combined fan plus intake calculation, the latter being represented via an axisymmetric approximation. With an initial prescribed velocity disturbance of the blades in a 2 nodal diameter mode, the calculations showed a strong response in a 4 nodal diameter mode. Considerable acoustic activity within the duct was also noted. This result was compared with CFD calculations for the full 3D intake geometry. It was concluded that a realistic representation of intake acoustics is required for a full description of the problem.

INTRODUCTION

Over the last ten years or so, measurements on aero-engine test rigs and theoretical considerations have lead to the hypothesis that fan flutter may be influenced by the acoustic properties of the intake duct. It has been postulated that the variation in the cross-sectional area of the duct may cause acoustic waves from the fan to be cut-off at the intake throat, the trapped energy leading to an acoustic resonance and to greater susceptibility to fan blade flutter (Parry 1995). The aim of the paper is to establish whether the intake duct properties play a significant enough role in flutter stability so that their inclusion into the numerical model is necessary. Previous related work was recently reported by Chew et al (1997) and Vahdati et al (1997).

A full review of intake acoustics is well beyond the scope of the present contribution but it is useful to mention some of the relevant publications. Studies of the acoustics of variable area ducts with quasi one-dimensional flow models have been carried out by Gupta et al. (1995) who used a segmentation approach. Campos & Lau (1996) assumed a low Mach number and that the acoustic wavelength was negligible compared to the length scale of the cross-sectional area variation, allowing them to derive an analytical solution. Uenishi & Myers (1984) used a two dimensional modified wave energy method (WEM) to represent the sound field in a non-uniform duct carrying a quasi one-dimensional mean flow. Eversman & Astley (1981) and Astley and Eversman (1981) used numerical methods to consider the transmission of sound through non-uniform ducts carrying high-speed compressible flows. Most of the relevant theoretical work in three dimensions has been carried out under the direction of Nayfeh who has used a mixture of analytical and numerical methods to study the acoustics of non-uniform circular and annular ducts with a range of mean flow profiles for both hard and soft wall boundary conditions (Nayfeh et al. 1975, 1979, 1980). The case of rotating blade rows has been investigated by Hanson (1993) who modified the flat plate cascade model of Smith (1972) to accommodate two blade rows in relative motion. His results showed that acoustic mode trapping could occur in such situations.

Very recently, Vahdati et al. (1997) reported the use of a 3D unsteady flow solver in the case of an actual intake geometry. At conditions representative of engine fan flutter, a build up of acoustic energy in the duct was observed for both hard and soft wall conditions. Such findings not only support the earlier hypothesis that an acoustic resonance in the intake duct may affect the fan stability and but also provide a closer quantitative agreement with engine observations than what was obtained from simpler one-dimensional calculations. In this previous study, the acoustic effects of the fan flutter were simulated via a pressure perturbation which

Presented at the International Gas Turbine & Aeroengine Congress & Exhibition
Stockholm, Sweden — June 2–June 5, 1998

was applied at the duct exit boundary. The pressure perturbation was chosen such that it had the expected flutter frequency and the associated nodal diameter mode shape[1]. It was therefore inherently assumed that any changes to the fan flutter condition due to the acoustic interactions from the intake duct are not modelled as the pressure perturbation is kept fixed throughout the calculations. Similar calculations will be reported below and these will be compared to results from a fully coupled fan plus intake calculation.

The paper by Chew et al (1997) is also particularly relevant to the present work, as it describes and gives justification for the fan flutter model used here. In this paper CFD-based models were applied to fan flutter and results compared with experimental data. A major conclusion from this work was that part-speed assembly mode flutter is susceptible to CFD analysis using an essentially inviscid unsteady model. However, the unsteady solution must represent a perturbation from a representative steady-state condition, and calculation of the steady-state condition did require a viscous analysis. Further details of this modelling approach will be given here.

The aeroelasticity code AU3D, developed at the Vibration University Technology Centre of Imperial College, was used throughout the computations. The CFD part of the code is based on a non-linear Navier-Stokes or Euler representation which is time accurate. AU3D employs an implicit time-stepping algorithm and 3D unstructured meshes of tetrahedral elements (Vahdati & Imregun 1994), a feature that allows the efficient modelling of complex geometries such as whole fan and intake duct assemblies. The structural part of the code is based on a modal model obtained from a standard FE program, the vibration modes being interpolated onto the aerodynamic mesh which is moved at each time step according to the structural motion. The information exchange between the two domains is therefore achieved via pressures and displacements.

INTAKE-ALONE CALCULATIONS

The computational domain and mesh for the intake-alone calculations is shown in **Fig. 1**, the geometry being that of a typical modern design. The intake outflow boundary is chosen to approximate to the fan face position and the mesh, which has about 50,000 points, expands a good distance away from the intake in the external flow. An inviscid flow model was used with appropriate slip boundary conditions on the duct walls. For steady flow calculations, a representative static pressure distribution, obtained from a throughflow model of the fan, was imposed at the duct exit. Farfield flow was assumed to have a zero angle of attack and small forward velocity (Mach number ≈ 0.1). For unsteady calculations, a pressure perturbation was applied at the duct exit as follows:

$$p = \bar{p} + \Delta p \sin\{N\phi + (\omega_f + N\Omega)t\} \qquad (1)$$

where $\bar{p}$ is the steady flow exit pressure, Δp is the perturbation amplitude, N denotes the nodal diameter of the travelling wave, ϕ is the circumferential co-ordinate, ω_f is the blade frequency, Ω is the fan speed, and t denotes time.

For an acoustically hard wall, zero penetration conditions apply at the walls. However, most intakes have acoustic liners, the properties of which can be represented using a complex impedance. The same approach was used here and further details can be found in Vahdati et al. (1977) who reported earlier results for the same intake geometry. The steady-state flow characteristics were computed for 70%, 75% and 80% speeds at a number of aerodynamic conditions and the predicted mass flow rates were found to be within 3% or less of the measured values. Examples of surface Mach number distributions are given in **Fig. 2** for the 70% speed case.

Acoustic Results

A series of unsteady calculations were first undertaken for the N=2 mode. Initial conditions were set to the steady-state flow solution and a perturbation amplitude $\Delta p = 0.005\bar{p}$ was specified in equation (1). After running for about 14 periods with hard walled boundary conditions, the acoustic liner model was activated and the calculation continued. Some hard-wall results are illustrated in **Fig. 3** which shows the non-dimensional pressure perturbation amplitude along the axial line at the top dead centre on the duct wall at 75% speed and near-flutter condition Three different mass-flow points were considered to cover a range of conditions for acoustic activity build up. There is considerable acoustic activity within the duct and a peak-to-peak pressure perturbation of 0.10 at the fan face is seen to double in magnitude. Although the addition of acoustic liners generally reduces the pressure amplitudes, this is not always the case as indicated by **Fig. 4** which shows the pressure time histories for the 70% and 75% speed cases. An examination of the perturbation energy flux through the duct plane indicates that the energy input to the duct reduces as the liner is switched on for the 75%, the situation being reversed for the 70% speed case. However, by scaling the results to the same acoustic energy flux, it was found that the addition of acoustic liners always reduced the unsteady pressure perturbations on the intake.

Further numerical experiments were conducted for the N=2 case, inputting a single pressure wave at the duct exit. The unsteady pressure was then imposed for one period at the duct exit before reverting to the usual exit boundary conditions. **Fig. 5** shows some results from these calculations. It is apparent that multiple reflections of the acoustic pulse occur, leading to a gradually decaying acoustic signal.

A limited number of results were obtained for the N=3 and N=4, forward travelling modes. Of particular note is the 70% speed case for N=4 in **Fig. 6**. The perturbation energy flux at the fan face was relatively low for this case, suggesting proximity to a resonant condition. However, the level of acoustic activity within the duct is less than that for the N=2 mode at the same flow condition (**Fig. 3**).

FAN ASSEMBLY PLUS INTAKE DUCT CALCULATIONS

As for the intake only studies, the AU3D code was used here. An axisymmetric approximation to the intake duct described above was employed as this simplification allowed calculations for the entire domain to be conducted on a mesh rotating with the fan. The fan geometry employed was a representative wide-chord civil aero-engine fan with 22 blades.

[1] Bladed assemblies vibrate in such a way that the contours of the stationary points coincide with the disk diameters, hence the term nodal diameter.

The flutter analysis procedure, developed at the Vibration UTC in the light of previous experience, was applied to the combined intake duct and fan assembly. The steps are given for the fan assembly only as the addition of the intake duct has no effect on the procedure. An application of the procedure to a different fan assembly is described by Chew et al (1997).

(i) Compute a steady-state viscous solution for a single blade passage using a fine mesh, so that important features such as shock strength and position can be captured as accurately as possible.

(ii) Use a second (coarser) mesh and model the whole annulus via an inviscid flow representation. (This step is required to reduce the computational effort and it is expected that it will be eliminated by increased use of parallelised codes and improved solution techniques). Adjust the inviscid whole annulus model using the results from the finer viscous mesh so that the steady-state solution is as similar as possible on both meshes. This is achieved by using the so-called loss model which forces the steady-state inviscid solution to equal the viscous result interpolated from the finer mesh, but neglects the unsteady viscous terms..

(iii) Obtain the first 5 or so blade vibration modes using a linear FE model. Expand the blade modes into assembly nodal diameter (ND) modes by assuming a rigid disk connection between the blades.

(iv) Interpolate the assembly modes onto the inviscid aerodynamic mesh, thus obtaining the aeroelastic mesh.

(v) Initiate the flutter calculation by giving an initial velocity in one or more modes. Move the aeroelastic mesh at each time step according to the structural assembly mode shape.

(vi) Assess flutter stability by inspecting the decaying or growing travelling wave time histories.

The main advantage of such an approach lies in the fact that all nodal diameter (or interblade phase angle) modes are present in the computation and energy exchanges between them are modelled automatically. The results are obtained from a single calculation and stability is assessed from individual modal time histories.

Steady Flow Predictions

The computational mesh for the single passage viscous steady-state solution is shown in **Fig. 7**. The mesh used has about 104,000 points and it is unstructured in the blade-to-blade (axial and tangential) plane but such 2D sections are stacked, thus forming a semi-unstructured grid as described by Sbardella et al (1997). The domain includes an axisymmetric representation of the intake, blending with a straight duct upstream. Owing to the mesh being stacked radially, it was necessary to include a thin tube on the centre-line. The calculations were performed at a 75% speed condition. The inflow and exit boundary conditions were specified via inlet total pressure, total temperature and flow angle, and exit static pressure distribution. The no-slip condition was applied on the blade surfaces using turbulent wall functions and the intake wall was treated as a 'slip' boundary so that calculation of the end wall boundary layer was not included. The steady-state solution was checked against the measured mass flow rate and the predicted value was found to be within 3% of the measured one. The pressure contours at the blade tip section are shown in **Fig. 8**. As usual for part-speed aerodynamic behaviour, the shock is expelled out of the passage and it intersects with the blade suction surface less than half a chord downstream of the leading edge. Further examination of the solution has shown that the shock decay upstream of the fan is more rapid than that expected from theory (e.g. Morfey and Fisher, 1970). This is to be expected for the mesh size used here. The question arises as to whether the interaction of the shock waves with the lower frequency acoustic waves associated with flutter, which will not be fully captured on this calculation mesh, is important. While this point is noted here, it remains unanswered. However, the primary aim of this study was to demonstrate the coupling of intake acoustics with fan flutter. Shock interaction may modify this coupling but is not seen as a primary cause.

Flutter Analysis

The domain and calculation mesh for the aeroelasticity analysis is shown in **Fig. 9**. To reduce the computational effort, only half of the 22-bladed fan assembly was included in the coarse inviscid mesh which contained about 112,000 points. The intake wall was treated as hard, i.e. no acoustic liner model was used. The procedure of Section 3.1 was followed for the flutter analysis but it should be noted that only the even nodal diameter modes are included in the computations because of using half the assembly. Also, although the first five modes were included in the calculations, only the first flap mode, at 86.5 Hz, was found to play a significant part. Since this particular fan was believed to flutter primarily in the 2 nodal diameter assembly mode, the calculation was initiated by giving an initial velocity in that mode.

The time histories of the forward and backward travelling assembly vibration modes are shown in **Fig. 10** for a time length of 0.35 seconds after the initial disturbance. The initial forward travelling 2 ND mode decays slightly over the period of the calculation but the backward 2 ND mode decays rapidly. An examination of other time histories reveals that there is some energy exchange between the various nodal diameter modes as the initial velocity disturbance which has a 2 ND pattern produces a response in other forward travelling modes such as 4, 6 and 8 ND modes, the case for the 4 ND mode being particularly pronounced. This somewhat unexpected behaviour, not usually present in fan only flutter analyses, suggests that the intake duct might be instrumental for coupling the 2 and 4 ND modes. No acoustic liners were used in this particular case and hence their potential for reducing the vibration amplitudes is not taken into account. Furthermore, given the non-linear nature of the aeroelasticity model, it is not clear how the time histories would behave if the solution was carried out for a much longer time.

Further insight into the solution is given by the instantaneous pressure perturbation plots of **Fig. 11**. These plots are obtained by computing the average pressure values over one vibration cycle and subtracting those from the actual instantaneous pressure distribution. Near the blades, large perturbations arise around the shocks. Also shown in **Fig 11** is the circumferential variation of the pressure perturbation over the half assembly, upstream of the fan. It is easily seen that the perturbations are dominated by the 4 ND mode which is identified as a forward travelling wave by animating the pressure perturbations. The growth of the 4 ND mode is considered to be associated with some acoustic activity in the intake duct, the exact mechanism of which is yet to be explained.

The peak-to-peak pressure perturbation amplitudes on the intake wall are plotted against axial distance in **Fig. 12** where the positions of the blade leading edge and the intake throat are also shown. Close to the fan, the pressure perturbations are dominated by

the shock perturbations. From an axial distance of about -1.4 m, the 4 ND forward travelling wave begins to dominate with almost constant amplitude up to the intake throat at x about -1.75, this being the region in which the steady state solution fails to propagate the shocks. Thereafter, there is a gradual decay of the pressure wave upstream of the throat. The duct alone calculations, reported in Section 2, show a different behaviour with stronger axial decay of the perturbation amplitude within the intake. Such differences might be due to the different intake entry conditions between the two cases, with the upstream duct used in the present model more likely to give reflections from the CFD boundary.

Comparison with Acoustic Theory

Parry (1995) postulated that when acoustic waves were cut on at the fan entry but cut off at the intake throat, energy would be trapped in the system and resonances might occur as a result. Here the cut on condition is estimated from elementary 1D acoustic theory (see, for example, Vahdati et al. 1997) and compared to the above CFD calculations. It is assumed that, locally, the geometry of the intake can be approximated to that of an infinite cylinder. The local pressure perturbation field at any axial position of the intake duct can then be expressed in terms of available analytical solutions for the case of uniform infinite cylinder with the same local radius. For the 75% speed case, the analytically-obtained results of such an approach are shown in **Fig. 13** which defines the stability boundaries for fan entry and intake throat positions. For each nodal diameter, the mass flow just sufficient to give a cut on condition has been calculated. Two different curves are obtained since the cut-on condition is a function of the local equivalent radius, which is different for the fan entry and the intake throat. The acoustic wave is cut on for mass flow rates greater than these critical values and cut off at lower mass flow rates. Using the mass flow range of the 3 conditions for the 75% speed condition, **Fig. 13** indicates resonance in 5 to 8 nodal diameters. Given the approximate nature of these calculations, the agreement with the CFD results is reasonable.

CONCLUDING REMARKS

(i) The results lend support to the view that fan flutter can be affected by the intake duct acoustics. This finding confirms that intake acoustics should be considered when modelling fan flutter.

(ii) For a hard walled, axisymmetric intake duct, an initial disturbance in the 2 ND mode is seen to initiate a duct response in the forward travelling 4 ND mode, a phenomenon which is considered to be due the interaction of fan assembly vibration with the intake duct acoustics. In practice, such behaviour is expected to be influenced strongly by the presence of acoustic liners. The behaviour may also be affected by asymmetric 3D duct geometries, the boundary conditions in the CFD calculations, the mesh density and full vs. half assembly models. Nevertheless, the result clearly demonstrates that such coupling effects are possible and can be obtained using available modelling methods.

(iii) The combined fan plus intake calculations are consistent with the intake only CFD calculations and elementary theory for duct acoustics. Further work is required to quantify the effects of non-axisymmetric intake ducts, acoustic liners and mesh resolution.

(iv) Finally, the findings need to be checked against available experimental evidence, though there is a lack of reliable data. Future rig and engine tests should address this issue.

ACKNOWLEDGEMENTS

The authors would like to thank Rolls-Royce plc for their support and allowing the publication of this paper. The help of colleagues at Rolls-Royce and Imperial College with various aspects of this work is also gratefully acknowledged. The authors also wish to thank the Ministry of Defence (MOD), Defence Evaluation and Research Agency (DERA) and the Department of Trade and Industry for their support for part of this work.

REFERENCES

Astley, R. J. & Eversman, W, 1981. Acoustic transmission in non-uniform ducts with mean flow. Part II The finite element method. JSV, Vol. 74, 103-121

Campos, L. M. B. C. & Lau, F. J. P, 1996. On the acoustics of low Mach number bulged, throated and baffled nozzles, JSV, Vol. 196, 611-633

Chew, J. W., Marshall, J. G., Vahdati, M. & Imregun, M.,1997. Part-speed flutter analysis of a wide-chord fan blade. Proc of 8th Int Symp. on Unsteady Aerodynamics & Aeroelasticity of Turbomachines, Stockholm, Sweden.

Evans, D. V. & Linton, C. M., 1994. Acoustic resonance in ducts, JSV, Vol. 173, 85-94

Eversman, W. & Astley, R. J., 1981. Acoustic transmission in non-uniform ducts with mean flow. Part I: the method of weighted residuals, JSV, Vol. 74, 89-101

Gupta, V. H., Easwaran, V. & Munjal, M. L., 1995. A modified segmentation approach for analysing plane wave propagation in non-uniform ducts with mean flow, JSV, Vol. 182, 697-707

Hanson, D. B., 1993. Mode trapping in coupled 2D cascade - acoustic and aerodynamic results, AIAA paper 93-4417

Melling, T.H., 1973. The acoustic impedance of perforates at medium and high sound pressure levels, JSV, Vol. 29, 1-65.

Morfey, C.L. & Fisher, M.J., 1970. Shock-wave radiation from a supersonic ducted rotor. Aero J of the Roy Aero Soc, 74, 579-585.

Nayfeh, A. H., Kaiser, J. E. & Telionis, D. P., 1975. Transmission of sound through annular ducts of varying cross sections, AIAA J., Vol. 13, 60-65

Nayfeh, A. H., Kaiser, J. E. & Shaker, B. S., 1979. A wave envelope analysis of sound propagation in non-uniform circular ducts with compressible mean flows, NASA contractor Report 3109

Nayfeh, A. H. Shaker, B. S. & Kaiser, J. E., 1980. Transmission of sound through non-uniform circular ducts with compressible mean flows, AIAA J, Vol. 18, 515-525

Nayfeh, A. H. & Telionis, D. P., 1973. Acoustic propagation in ducts with varying cross sections, J. Acoustical Society of America, Vol. 54, 1654-1661

Parker, R. & Stoneman, S. A. T, 1989. The excitation and consequences of acoustic resonances in enclosed fluid flow around solid bodies, Proc. Inst. Mech. Eng, Vol. 203, pp 9-19

Parry, A. B., 1995. A possible link between fan flutter and an acoustic resonance of the intake system, Rolls-Royce Memorandum

Sbardella, L, Sayma, A. I. & Imregun, M.,1997. A semi-unstructured mesh generator for flow calculations in axial turbomachinery blading. Proc. 8th International Symposium on

Unsteady Aerodynamics and Aeroelasticity of Turbomachines, Stockholm, Sweden.

Smith, S. N., 1972. Discrete frequency generation in axial flow turbomachines, ARC R&M 3079

Vahdati, M., Chew, J.W., Parry, A. B. & Imregun, M. 1997. A study of intake duct acoustic resonance at fan flutter frequencies. Submitted to JSV

Vahdati, M. & Imregun, M., 1994. Non-linear Aeroelasticity Analyses using unstructured dynamic meshes. Proc. 7th Symp. Unsteady Aerodynamics and Aeroelasticity of Turbomachines, Fukuoka, Japan.

Uenishi, K. & Myers, M. K., 1984. Two-dimensional acoustic field in a non-uniform duct carrying compressible flow, AIAA J., Vol. 22, pp 1242-1248

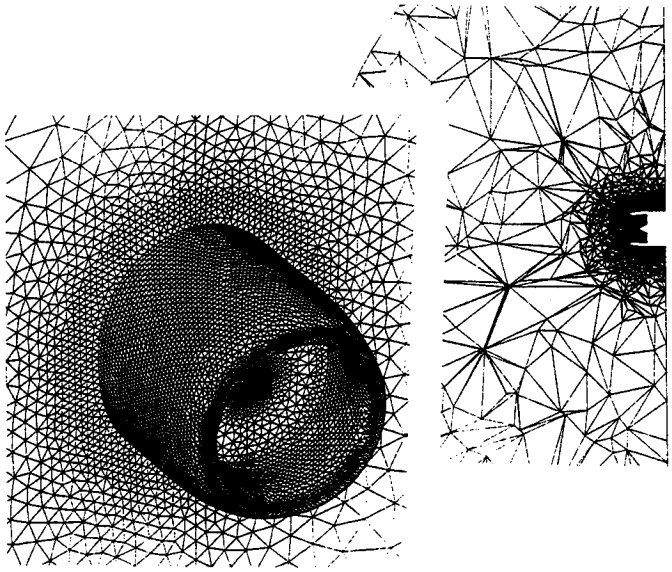

Fig. 1 Computational mesh for the intake-alone calculations

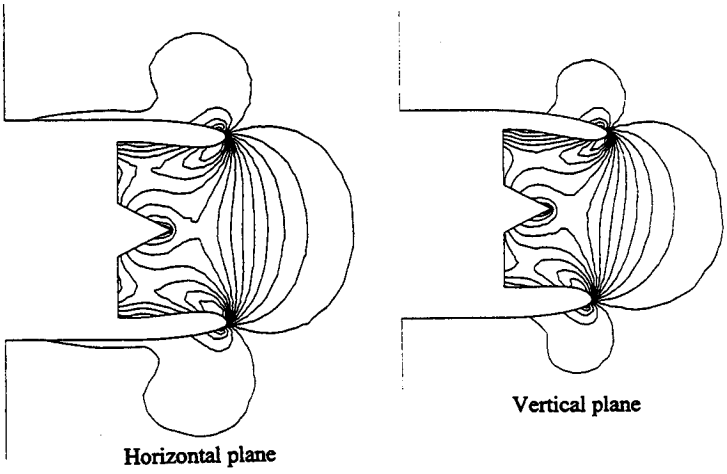

Fig. 2 Duct Mach number contours for 70% speed

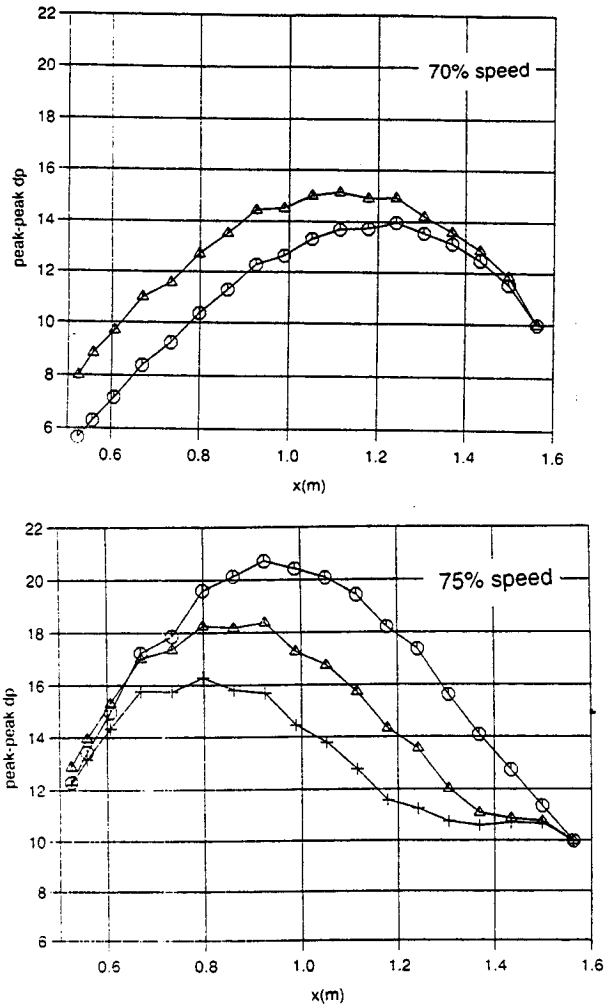

Fig. 3 Variation of the pressure perturbation with distance
70% speed - 2 aerodynamic conditions
75% speed - 3 aerodynamic conditions

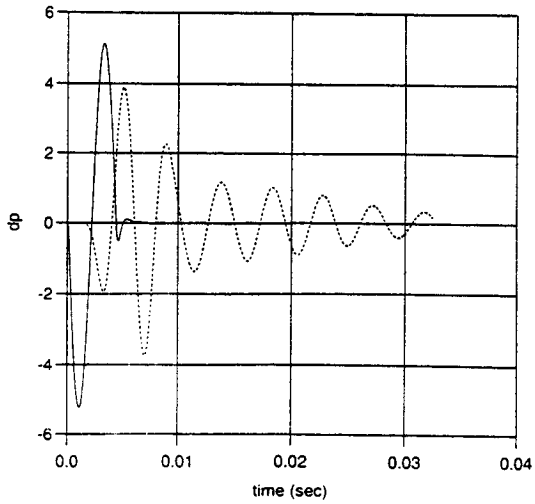

Fig. 5 Duct pressure time history at 75% speed
____ fan entry, ... mid-axial position

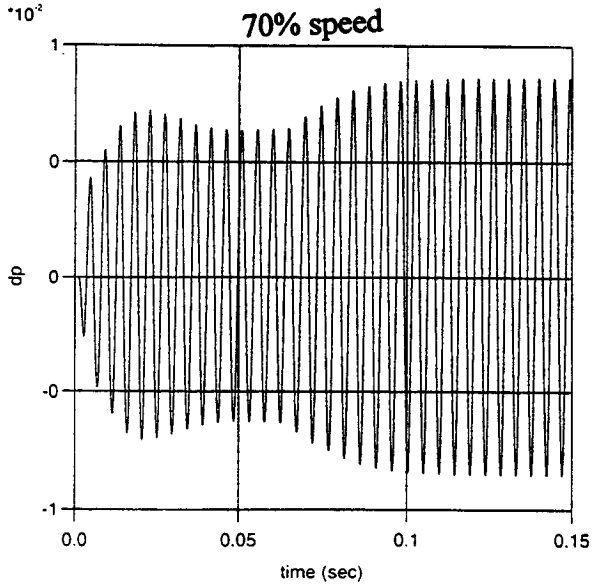

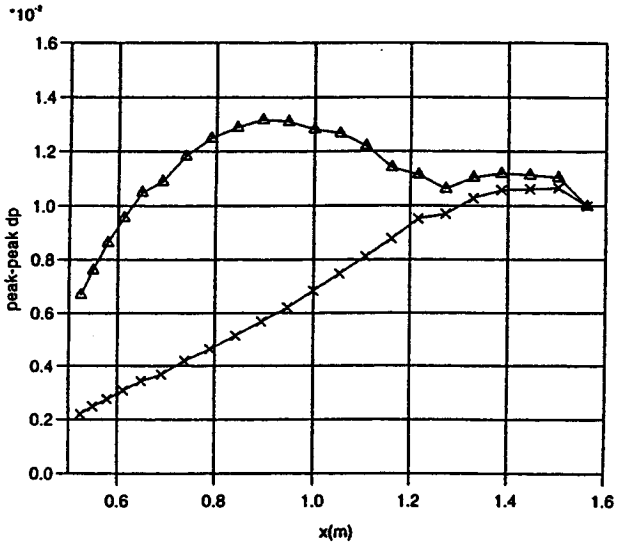

Fig. 6 Variation of pressure perturbation with distance
N=4, x=70% speed, Δ=75% speed

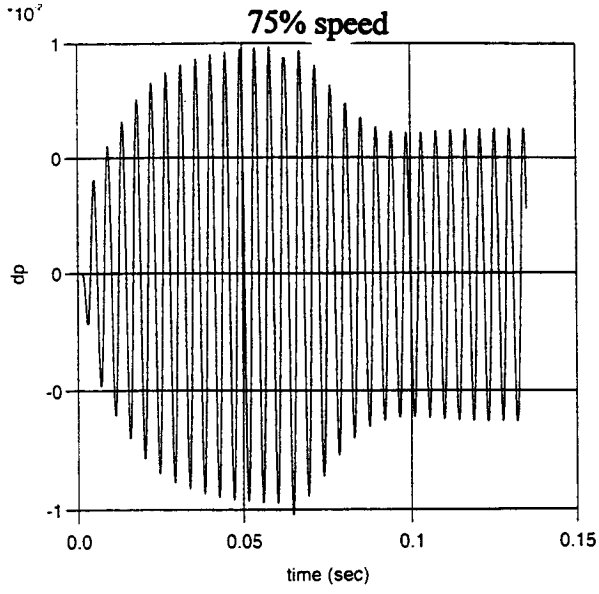

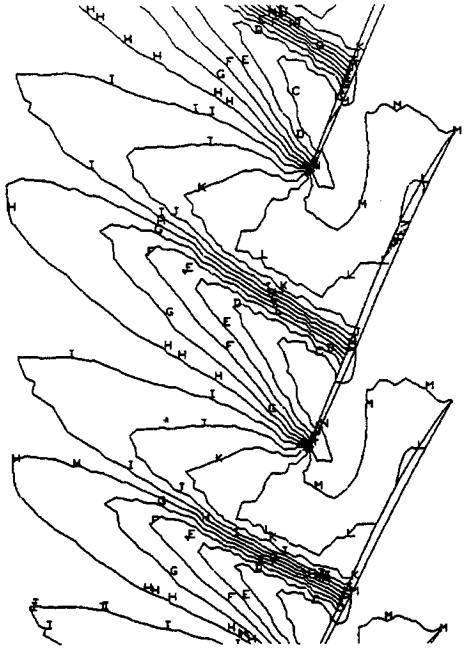

Fig. 4 Pressure perturbation time histories
The liner is switched on after about 0.065 seconds

Fig. 8 Pressure contours from steady-state plus intake calculations

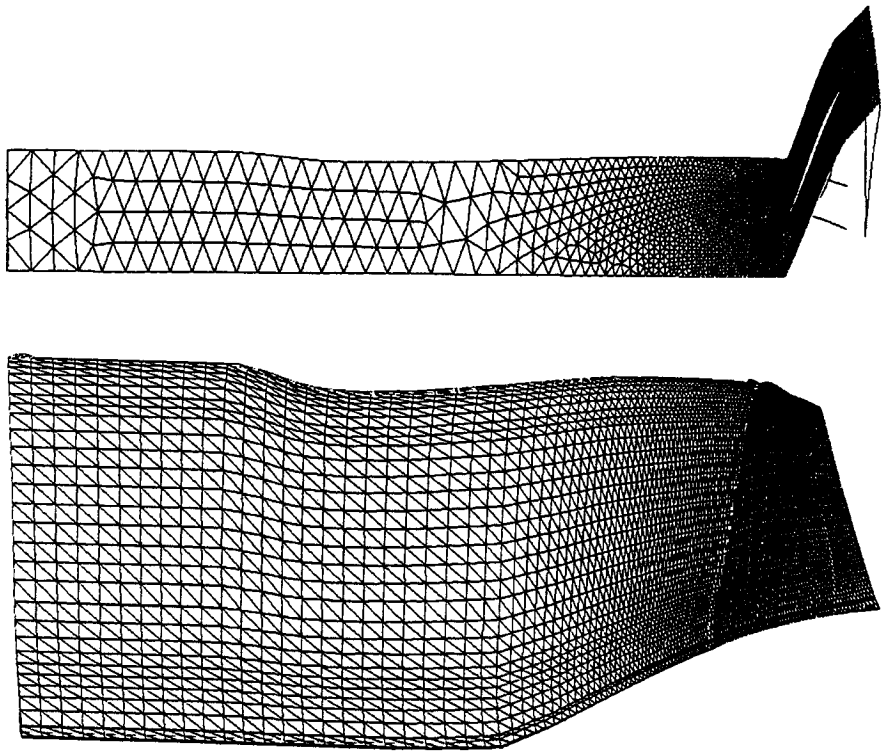

Fig. 7 Computational mesh for fan plus intake calculations - steady-state

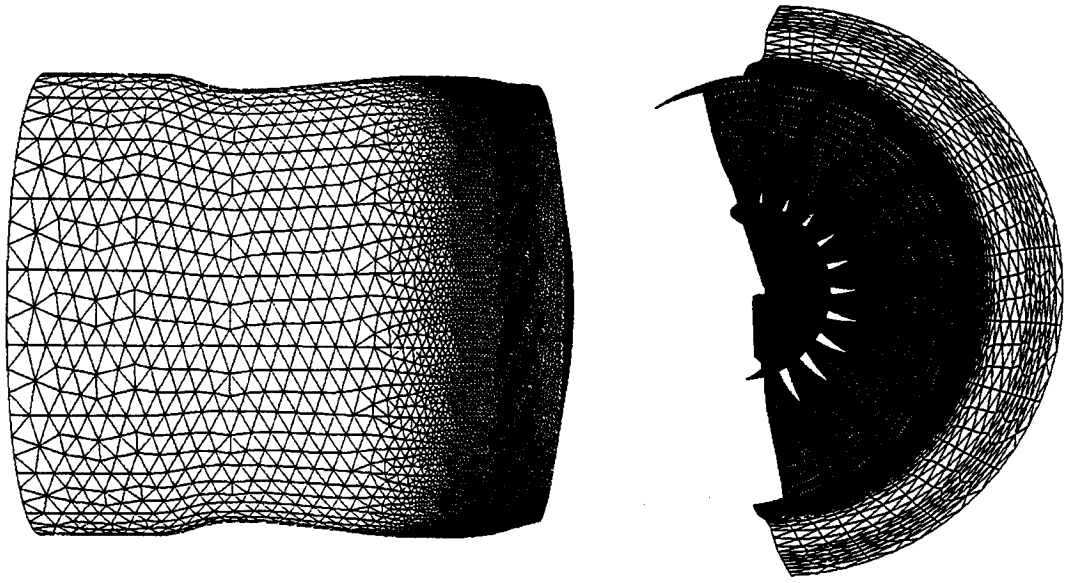

Fig. 9 Computational mesh for fan plus intake calculations - unsteady

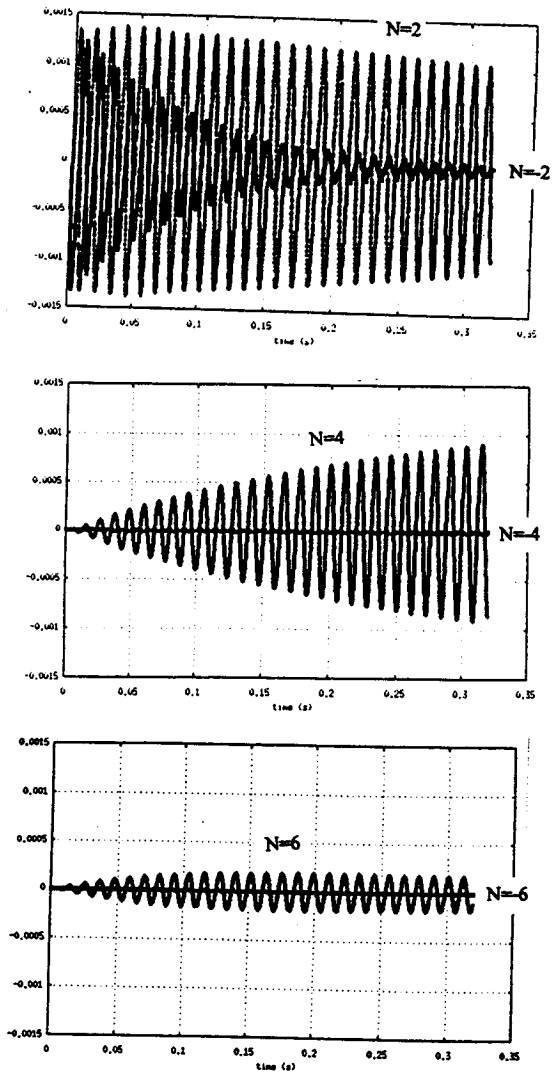

Fig. 10 First flap modal time histories from fan plus intake calculations

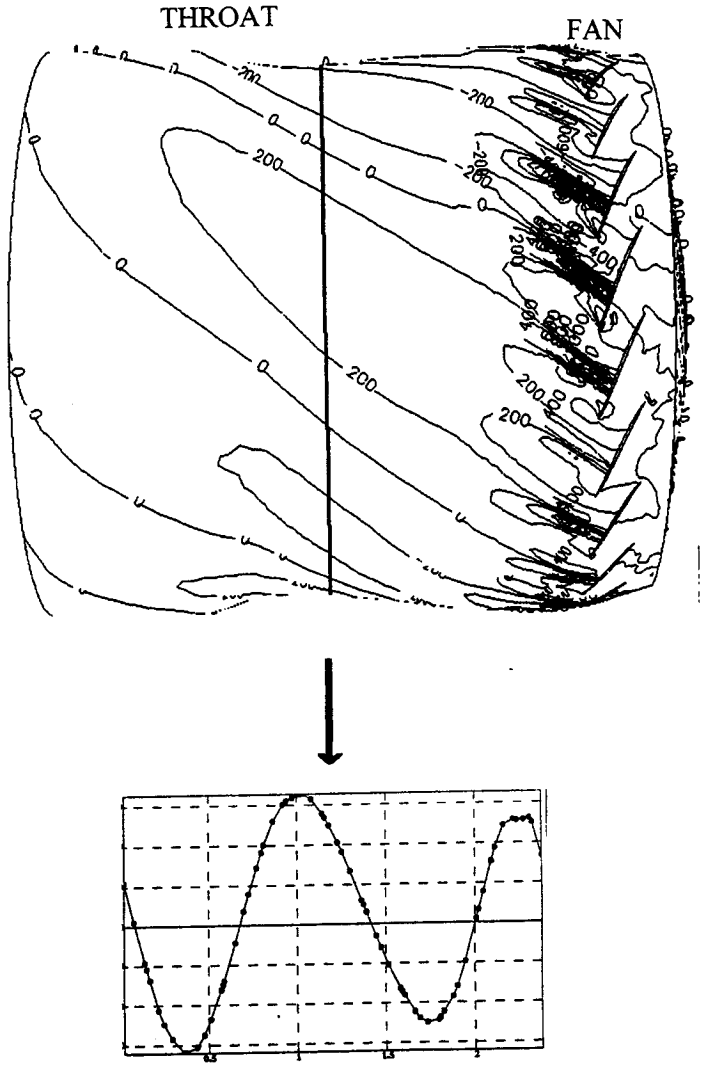

Fig. 11 Instantaneous pressure perturbations from fan plus intake calculations

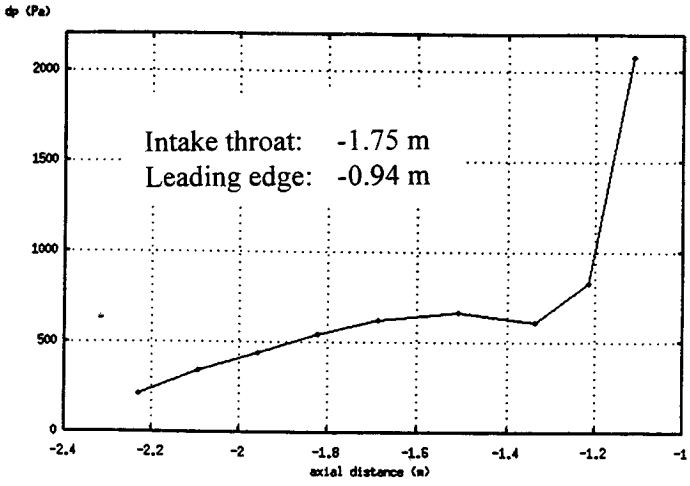

Fig. 12 Peak-to-peak unsteady pressure perturbations on the duct wall

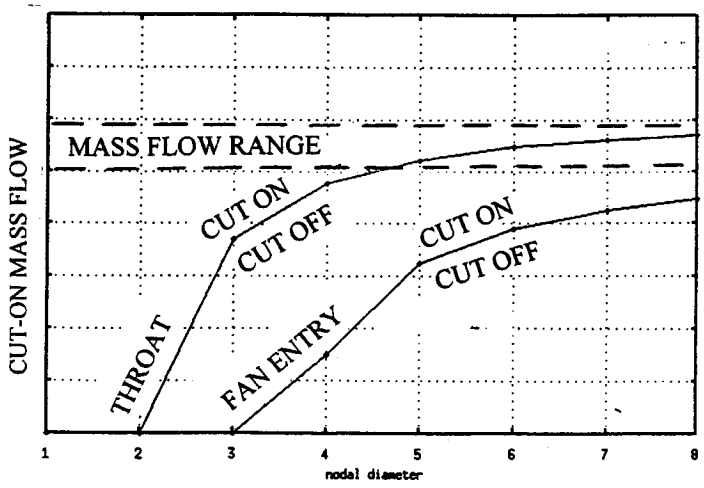

Fig. 13 Cut-on conditions estimated from acoustic theory 75% speed